

# MnO-Co@Pt nanowires encapsulated in N-doped porous carbon derived from MOFs for efficient electrocatalytic activity in methanol oxidation reaction

Shokhrukhbek Askarov, Yujing Ren, Tong Wang, Yunqi Yu, Salman Khan, Yaoyuan Zhang, Kangcheng Chen, Daxin Shi, Qin Wu and Hansheng Li \*

School of Chemistry and Chemical Engineering, Beijing Institute of Technology,

Beijing, 100081, China

\*Corresponding authors E-mail: hanshengli@bit.edu.cn; chenkc@bit.edu.cn; wuqin\_bit@126.com

## Experimental section

### Chemicals and reagents

Chloroplatinic acid ( $\text{H}_2\text{PtCl}_6 \cdot 6\text{H}_2\text{O}$ ), 2-Methylimidazole ( $\text{C}_4\text{H}_6\text{N}_2$ ), Cobalt nitrate hexahydrate ( $\text{Co}(\text{NO}_3)_2 \cdot 6\text{H}_2\text{O}$ ) from Aladdin Biochemical Technology Co., Ltd.  $\text{CH}_3\text{OH}$  and  $\text{C}_2\text{H}_5\text{OH}$  from Sinopharm Group, Purified water, Nafion (5 wt%) solution from Alfa Aesar Chemical Co., Ltd, Pt/C (20 wt%) from Johnson Matthey Company, Manganese (II) acetate tetrahydrate ( $(\text{CH}_3\text{COO})_2\text{Mn} \cdot 4\text{H}_2\text{O}$ ) and Trimesic acid ( $\text{H}_3\text{BTC}$ ) from Macklin Company. All chemicals were of high-purity analytical reagent grade and were directly used to prepare samples.

### Preparation of Mn-BTC

For the synthesis of Mn-BTC, previously reported procedure was employed with certain modifications<sup>1</sup>. Firstly, the 2.15 g of  $\text{H}_3\text{BTC}$  was dissolved in 250 mL distilled water and was stirred via magnetic stirring in the oil bath at 80 °C for 30 min (Solution A). Also,  $(\text{CH}_3\text{COO})_2\text{Mn} \cdot 4\text{H}_2\text{O}$  was dispersed in 250 mL distilled water, and heated at 80 °C for 30 min (Solution B). Following that, Solution B was mixed with Solution A and kept stirring at 80 °C for 5 h. Obtained white precipitates were washed 3 times with  $\text{CH}_3\text{OH}$  and centrifugated at 8000 rpm for 6 min. The obtained white precipitates were dried in a vacuum oven at 80 °C for 2 h.

### Preparation of Mn-BTC@ZIF-67

During the synthesis of Mn-BTC@ZIF-67, the crystal size of ZIF-67 was controlled by the Solvent Effects. The solvent used during synthesis can have a significant impact on the final particle size of the material. Different solvents interact with the precursor molecules in different ways, affecting the nucleation and crystal growth processes. Specifically, the molar ratio among  $\text{Co}(\text{NO}_3)_2 \cdot 6\text{H}_2\text{O}$ , and 2-methylimidazole was kept constant at 1:46.5 and amounts of methanol in

the synthesis were adjusted based on its molar ratio to  $\text{Co}^{2+}$  to prepare different sizes ZIF-67 crystals on Mn-BTC precursor. As-synthesized 0.1g Mn-BTC white powder was added into 50 mL  $\text{CH}_3\text{OH}$  (Solution C), and sonication for 30 min was carried out to completely dissolve. Then, 1.64 g 2-Methylimidazole was added to Solution C and stirred at 35 °C for 30 min. Also, 0.125 g  $\text{Co}(\text{NO}_3)_2 \cdot 6\text{H}_2\text{O}$  was dissolved in 10 mL  $\text{CH}_3\text{OH}$  (Solution D) and stirred for 1 h. After, Solution D was quickly added to Solution C and continued stirring for 10 h. The obtained white-purple samples were 3 times washed with  $\text{CH}_3\text{OH}$  and centrifugated. Further, the obtained sample was dried in a vacuum oven at 80 °C for 2 h.

### **Preparation of MnO-Co@Pt NPC**

Mn-BTC@ZIF-67 MOFs-based nanocomposites 0.1 g were calcined at 800 °C for 2 h in the Ar atmosphere to prepare MnO-Co NPC (designated as MnO-Co NPC 800). Furthermore, MnO-Co NPC 800 was quickly mixed with 0.2 g  $\text{H}_2\text{PtCl}_6 \cdot 6\text{H}_2\text{O}$  and 7.62 g  $\text{CH}_3\text{OH}$  solution, and subsequent to ultrasonicated for 15 min, the resulting solution was centrifugated and washed with  $\text{CH}_3\text{OH}$ . Afterward, it was dried at room temperature for 1h in the vacuum oven. Finally, the obtained MnO-Co@Pt NPC 800 was designated as (MnO-Co@Pt NPC 800 15%).

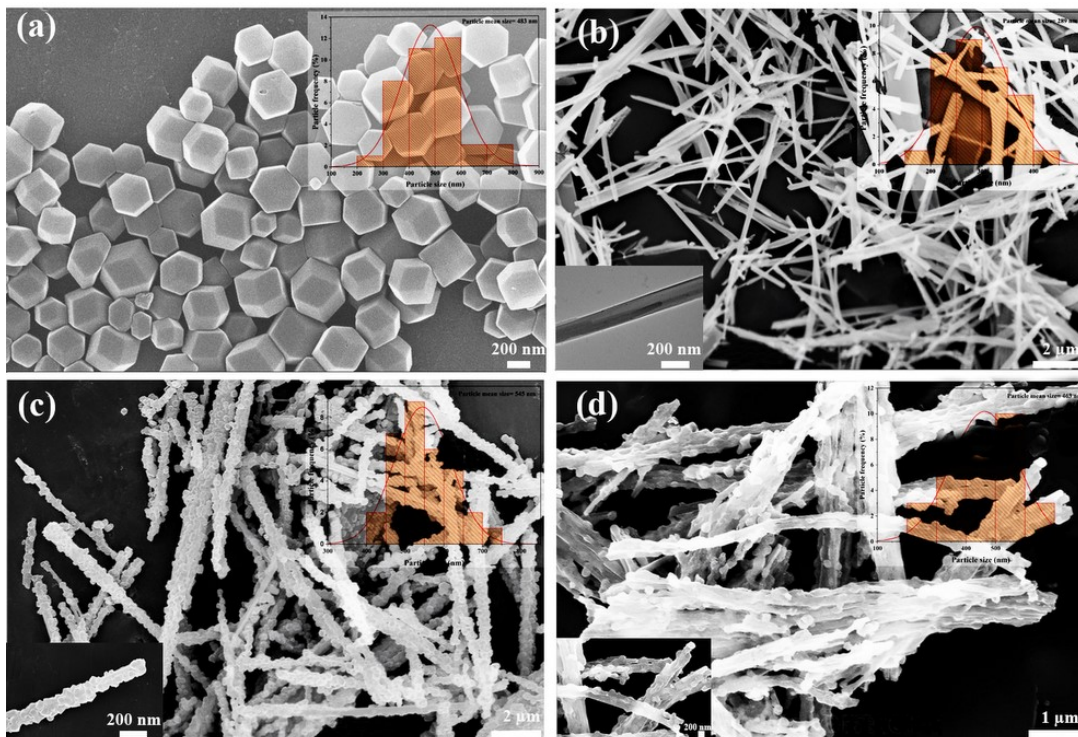
### **Characterizations**

A spectrum FTIR analyzer produced by Perkin-Elmer was employed to characterize the various groups of functional elements contained in the prepared samples. The crystal structures of the supports and catalysts were determined by X-ray powder diffraction (XRD) investigated on a Rigaku Ultima IV which has  $\text{Cu-K}\alpha$  radiation by Neo Science Company, Japan. The amount of metal has been analyzed by an inductively connected plasma-optical emission spectrometer (ICP-OES, Agilent725ES). The external morphology and structure of each sample were observed through a scanning electron microscope (SEM, Hitachi S4800). The internal morphology and structure of the samples were investigated by transmission electron microscope (TEM JEM1200EX) was employed. Furthermore, High-resolution TEM (HR-TEM) images and the corresponding energy-dispersive X-ray spectroscopy mapping images, elemental line, and the selected area electron diffraction (SAED) images were obtained via Talos F200X analytical electron microscope. Raman characterizes the disarray and the graphitization process levels of the samples were analyzed by LabRam HR Evolution; Horiba Scientific. The  $\text{N}_2$  adsorption-desorption experiment carried out at 77K is used to measure the pore size and the surface area (AUTOSORB IQ). TG graphs were analyzed by thermogravimetric analysis (TGA, WCT-1D) from 30 °C to 1000 °C, and temperature-programmed decomposition (TPD) was employed to analyze the thermal reactions of the samples. The treatment method of the TPR is as follows: The sample was heated from 25 °C to 100 °C by 10 °C/min; after maintaining the heat for 30 min at 100 °C, the temperature continues to rise to 1000 °C by 10 °C/min, followed by a gradual cooling process, and a heat conductivity analyzer was applied to identify the shift in atmospheric composition and

outgoing data, which were applied for calculating the products decomposition temperature. X-ray photoelectron spectrometry (XPS) is employed for identifying the surface elemental content and electrical structure of the elements.

### **Electrochemical measurements**

Electrochemical tests were also performed out with a CHI760D electrochemical workstation with a standard three-electrode system, Pt (counter) electrode, saturated calomel (reference) electrode, and a glassy carbon (working) electrode with 5 mm in diameter covered with a catalyst layer. For the preparation of the catalyst ink, 4.0 mg of catalyst was mixed with 500  $\mu\text{l}$  ethanol, 480  $\mu\text{l}$  water, and 10  $\mu\text{l}$  Nafion solution by ultrasonic for 1 h. Subsequently, 10  $\mu\text{l}$  of the prepared suspension was deposited on the surface of the glassy carbon electrode (GCE) and dried at room temperature. Also, the test temperature was 25  $^{\circ}\text{C}$ . The MOR performance was evaluated in an 0.5 M  $\text{CH}_3\text{OH}$ +0.5 M  $\text{H}_2\text{SO}_4$  solution scanned from -0.24 V to 0.96 V (vs. SCE). The electrochemical surface area (ECSA) calculated with the formula  $\text{ECSA} = \text{QH}/(0.21M_{\text{Pt}})$  was determined by the hydrogen adsorption/ desorption peaks of the cyclic voltammograms (CV) curves in an acidic medium. In the formula above, QH and  $M_{\text{Pt}}$  represented the charge of hydrogen adsorption/desorption ( $\text{mC cm}^{-2}$ ) and the loading of Pt ( $\text{mg cm}^{-2}$ ) of the working electrode and 0.21 denoted the charge which was connected with the monolayer adsorption of hydrogen on bright Pt. The chronoamperometry test was also performed to determine the stability of the catalyst at 0.65 V vs. SCE for 3600 s. The current densities that were obtained by the chronoamperometric measurement at 0.1 s and 3600 s were abbreviated to  $j_{0.1}$  and  $j_{3600}$ , and the retention rate was calculated by following  $(j_{3600}/j_{0.1}) * 100$ . Moreover, the CO-stripping measurements are concerned, the catalyst-modified GCE was immersed within a 0.5 M  $\text{H}_2\text{SO}_4$  solution for 30 min at -0.2 V. To ensure that the catalyst was fully poisoned by CO, the CO gas was bubbled into the solution for 30 min, and the CV curves were recorded (vs. SCE) scanning rate of  $100 \text{ mV}\cdot\text{s}^{-1}$ .<sup>2</sup>



(a) ZIF-67, (b) Mn-BTC@ZIF-67, (c) Mn-BTC, (d) MnO-Co@Pt NPC.

F  
ig.  
S1.  
SEM  
ima  
ges  
of (a)  
ZIF-  
67.

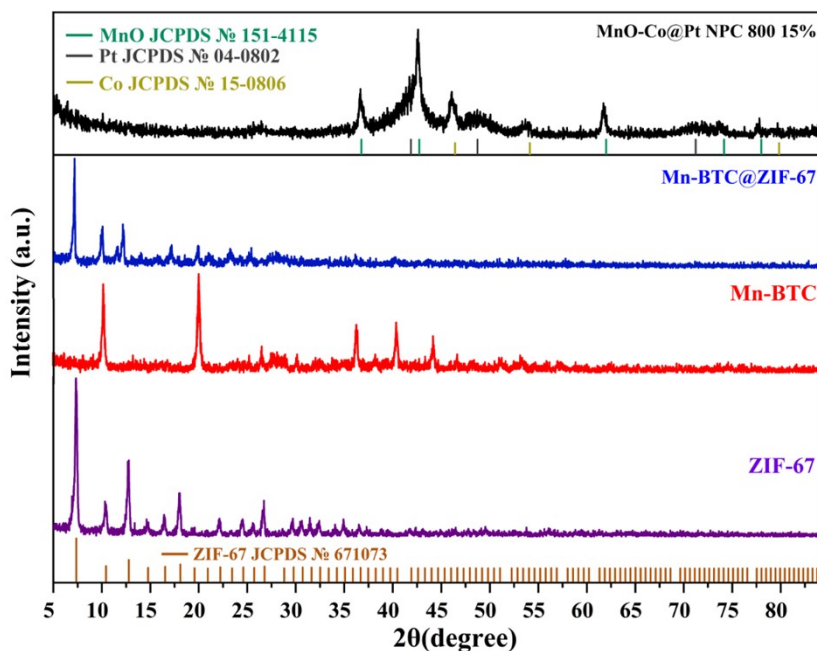
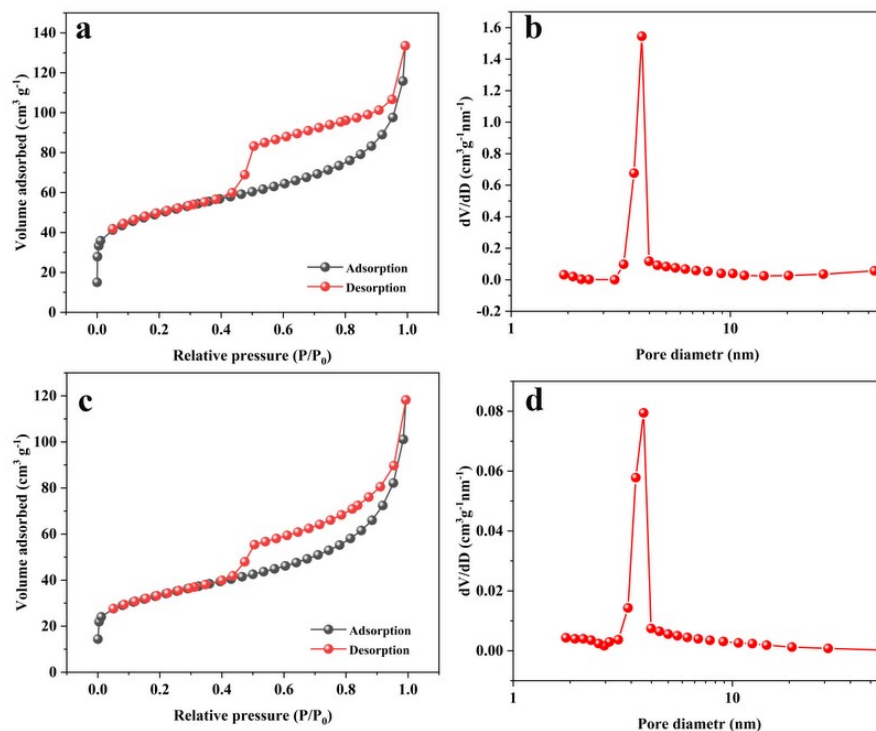
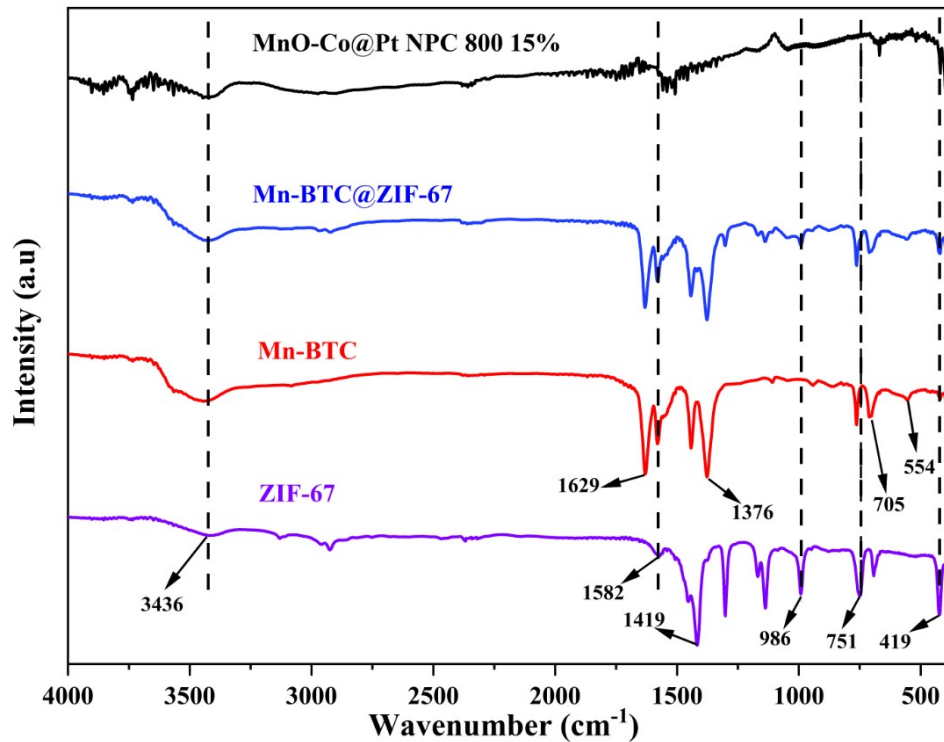


Fig. S2. XRD patterns of ZIF-67, Mn-BTC, Mn-BTC@ZIF-67, and MnO-Co@Pt NPC 800 15%.



**Fig. S3.** (a and c) N<sub>2</sub> adsorption-desorption isotherms and pore size distribution of MnO-Co@Pt NPC 700 and 900. (b and d) pore distribution curves.



**Fig. S4** FTIR patterns of ZIF-67, Mn-BTC, Mn-BTC@ZIF-67, and MnO-Co@Pt NPC 800 15%.

**Table S1.** Elements wt% in catalysts obtained from ICP-OES measurement.

Samples	Mn Wt%	Co Wt%	Pt Wt%	NPC Wt%	Pt/Mn	Pt/Co	Mn/Co
MnO-Co@Pt NPC 700 15%.	10.15	8.35	10.95	70.55	1.07882	1.31138	1.21557
MnO-Co@Pt NPC 800 10%.	10.1	7.65	5.95	76.3	0.58911	0.77778	1.32026
MnO-Co@Pt NPC 800 15%.	9.1	7.05	9.85	74	1.08242	1.39716	1.29078
MnO-Co@Pt NPC 800 20%.	12.4	7.5	15.45	70.2	2.25547	2.06	0.91333
MnO-Co@Pt NPC 900 15%.	8.75	8.05	12.35	70.85	1.41143	1.53416	1.08696

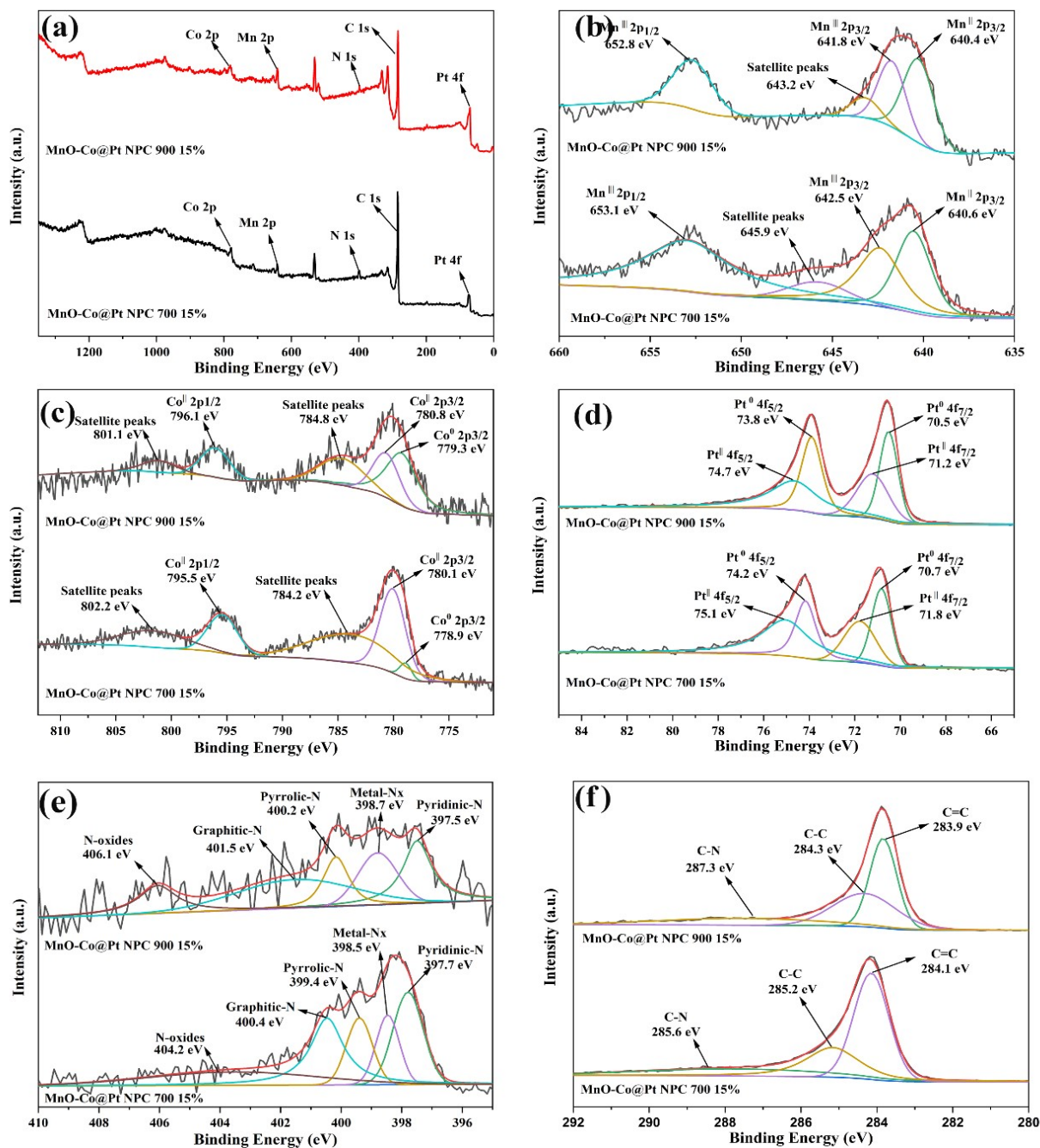


**Fig.S5** (a) XPS survey, (b) Mn 2p, (c) Co2p, (d) Pt 4f, (e) N 1s, and (f) C 1s XPS spectra of MnO-Co@Pt NPC 700 and 900 15%.

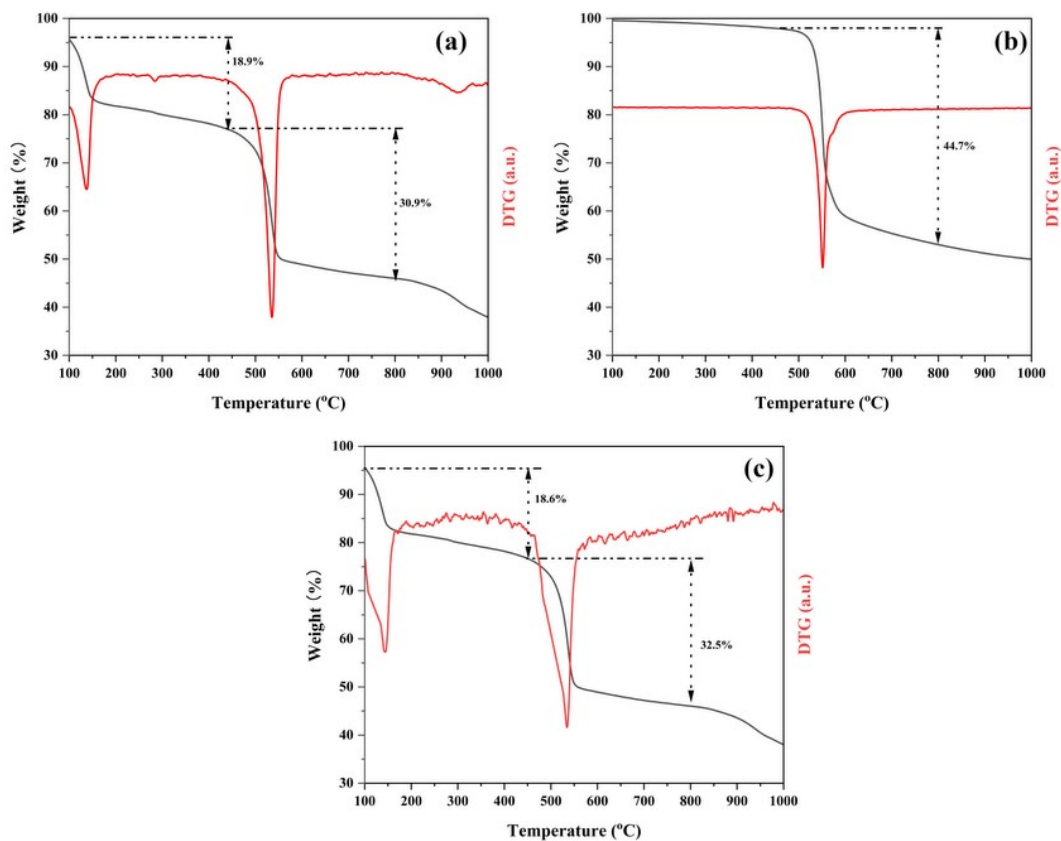


**Fig. S6.**  
images of  
BTC, (b)  
Mn-  
67.

TGA/DTA  
(a) Mn-  
ZIF-67, (c)  
BTC@ZIF-

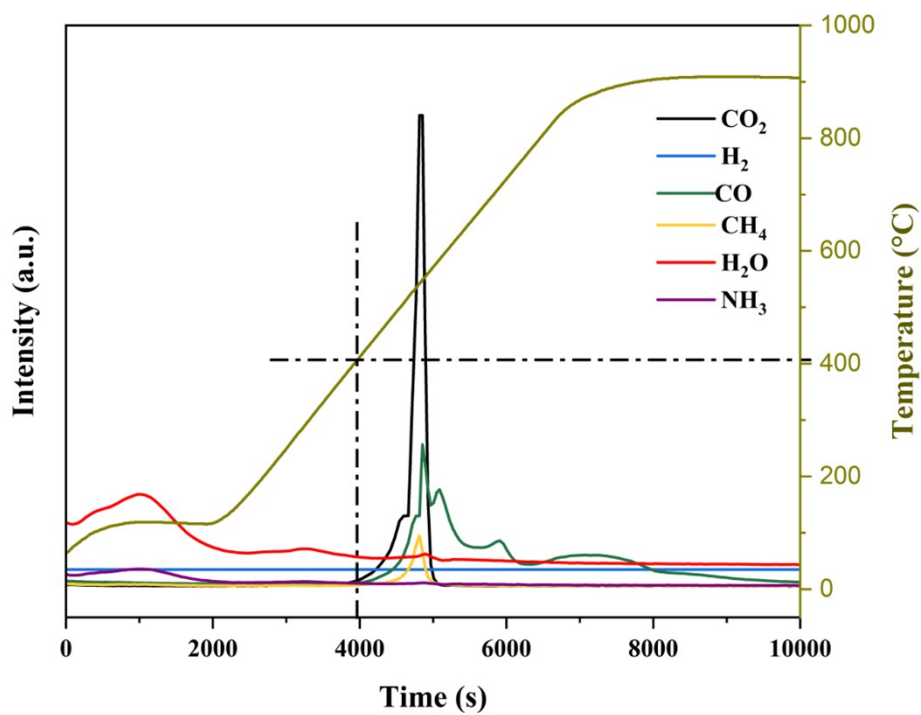


**Fig. S7.** Temperature-programmed decomposition (TPD) curves of MnO-Co NPC.

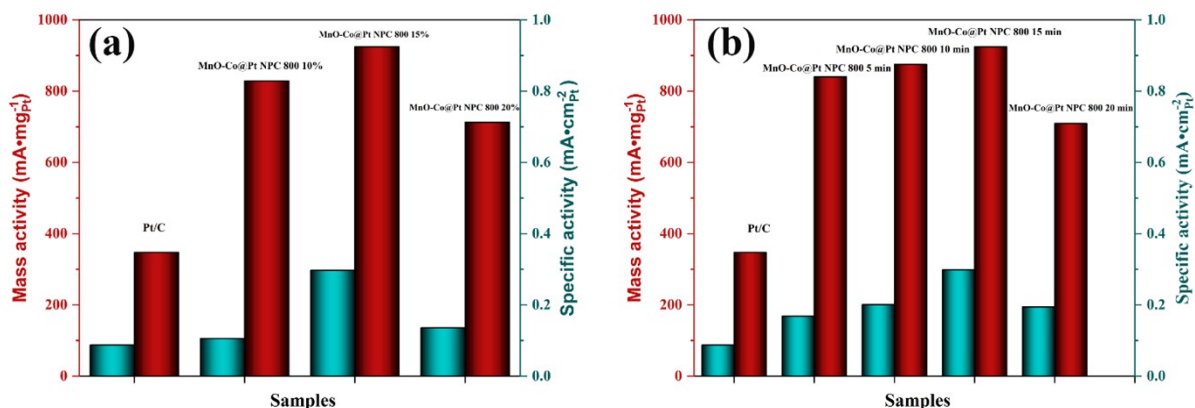


**Fig. S8.** (a) Mass activity and ECSA comparison of MnO-Co@Pt NPC 800 different Pt w%. (b) Mass activity and ECSA comparison of MnO-Co@Pt NPC 800 15% different galvanic replacement time.

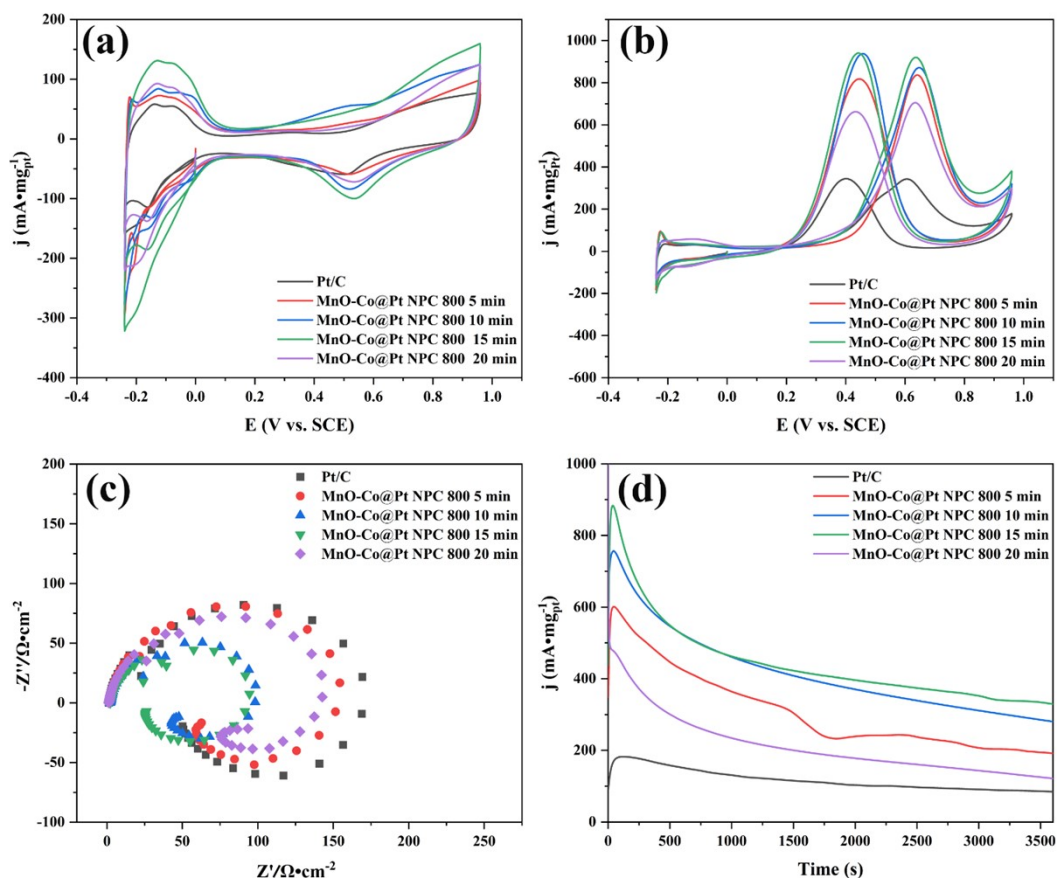


**Fig. S9.** (a) CV curves of catalysts in 0.5 M H<sub>2</sub>SO<sub>4</sub> at a scanning rate of 50 mV s<sup>-1</sup>, (b) CV curves of catalysts in 0.5 M H<sub>2</sub>SO<sub>4</sub> + 0.5 M CH<sub>3</sub>OH at a scan rate of 50 mV s<sup>-1</sup>, (c) Nyquist plots of catalysts, (d) Chronoamperometric curves of catalysts in 0.5 M H<sub>2</sub>SO<sub>4</sub>+0.5 M CH<sub>3</sub>OH at 0.65 V of MnO-Co@Pt NPC 800 15% different galvanic replacement time.

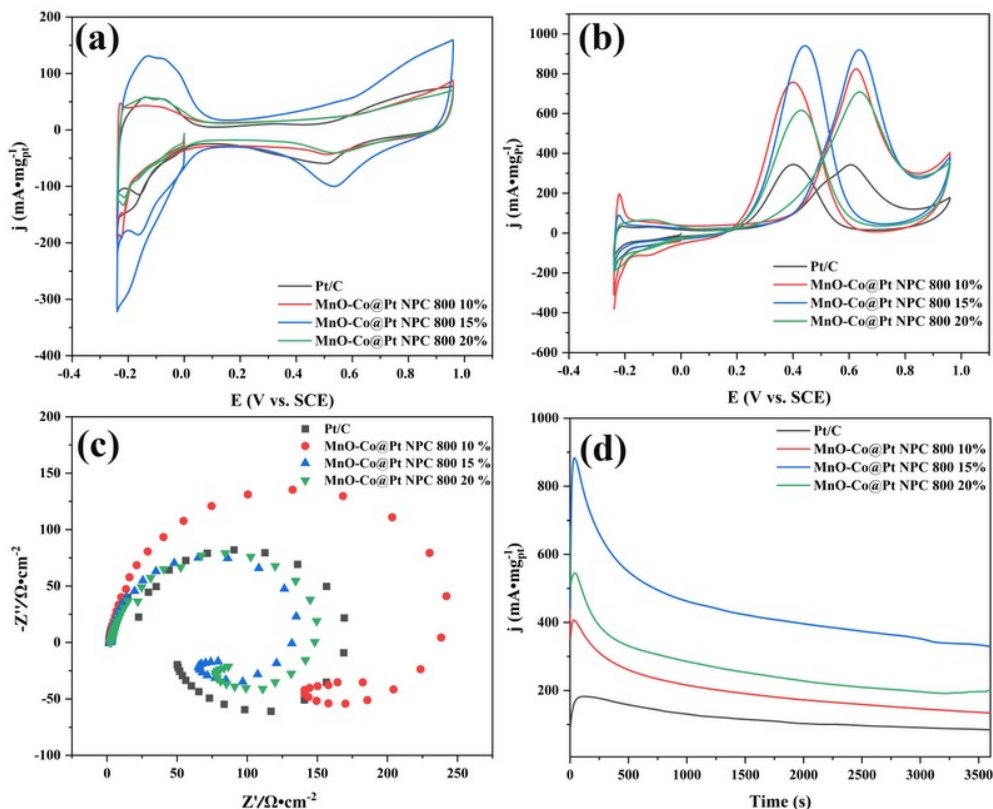


**Fig. S10.** (a) CV curves of catalysts in 0.5 M H<sub>2</sub>SO<sub>4</sub> at a scanning rate of 50 mV s<sup>-1</sup>, (b) CV curves of catalysts in 0.5 M H<sub>2</sub>SO<sub>4</sub> + 0.5 M CH<sub>3</sub>OH at a scan rate of 50 mV s<sup>-1</sup>, (c) Nyquist plots of catalysts, (d) Chronoamperometric curves of catalysts in 0.5 M H<sub>2</sub>SO<sub>4</sub>+0.5 M CH<sub>3</sub>OH at 0.65 V of MnO-Co@Pt NPC 800 different Pt w%.

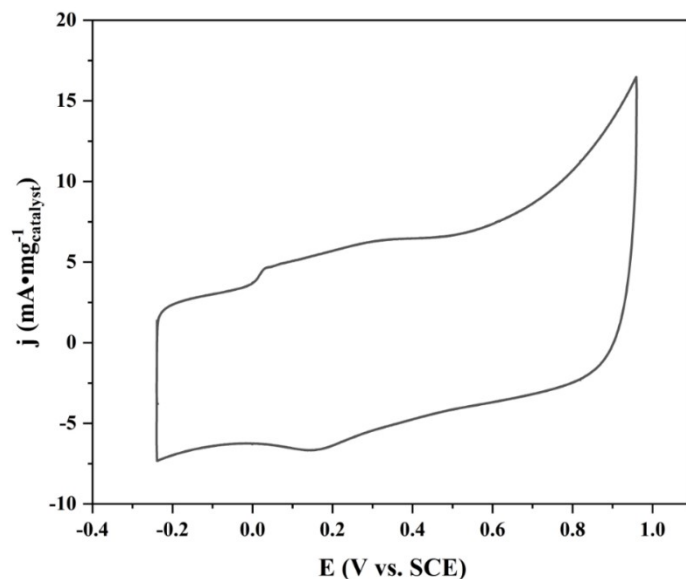


**Fig. S11.** CV curves of MnO-Co NPC in 0.5 M H<sub>2</sub>SO<sub>4</sub> + 0.5 M CH<sub>3</sub>OH at a scan rate of 50 mV s<sup>-1</sup>.

**Table S2.** Comparison of methanol oxidation performance on the MnO-Co@Pt NPC 800 nanocomposite with another Pt-based electrocatalysts.

Catalysts	Electrolyte	ECSA (m <sup>2</sup> g <sub>pt</sub> <sup>-1</sup> )	Mass activity (A mg <sub>pt</sub> <sup>-1</sup> )	Scan Rate (mV/s <sup>1</sup> )	Ref.
MnO-Co@Pt NPC 800	0.5 M H <sub>2</sub> SO <sub>4</sub> + 0.5 M CH <sub>3</sub> OH	280.0 5	0.924	50	This work
CoFe@Pt-NCs-X0.5-T700-t0	0.5 M H <sub>2</sub> SO <sub>4</sub> + 0.5 M CH <sub>3</sub> OH	93.5	0.915	50	3
Pt/Co/N-PC/N-CNTs	0.5 M H <sub>2</sub> SO <sub>4</sub> + 0.5 M CH <sub>3</sub> OH	76.79	0.583	50	4
Pt <sub>60</sub> Mn <sub>1.7</sub> Co <sub>38.3</sub>	0.5 M H <sub>2</sub> SO <sub>4</sub> + 1 M CH <sub>3</sub> OH	17	0.67	50	5
FePtPd nanowires	0.5 M H <sub>2</sub> SO <sub>4</sub> + 0.5 M CH <sub>3</sub> OH	N. A	0.49	50	6
PtRu-CoP/C-40%	0.5 M H <sub>2</sub> SO <sub>4</sub> + 1 M CH <sub>3</sub> OH	116.1 1	0.67	50	7
Pt <sub>66</sub> Au <sub>11</sub> Ni <sub>23</sub>	0.5 M H <sub>2</sub> SO <sub>4</sub> + 0.5 M CH <sub>3</sub> OH	44	0.228	50	8
np-PtRuCuW	0.5 M H <sub>2</sub> SO <sub>4</sub> + 0.5 M CH <sub>3</sub> OH	26	0.467	50	9
PtPdRu-3D	0.1 M H <sub>2</sub> SO <sub>4</sub> + 0.5 M CH <sub>3</sub> OH	156.6	0.436	50	10
PtPdCu-TiN	0.5 M H <sub>2</sub> SO <sub>4</sub> + 0.5 M CH <sub>3</sub> OH	76.2	0.366	50	11
PtPdCu cubic nanoframes	0.5 M H <sub>2</sub> SO <sub>4</sub> + 0.5 M CH <sub>3</sub> OH	51.5	0.455	50	12
Pt <sub>66</sub> Ni <sub>27</sub> Ru <sub>7</sub> DNSs	0.5 M H <sub>2</sub> SO <sub>4</sub> + 1 M CH <sub>3</sub> OH	19.9	0.805	50	13
Pt <sub>2</sub> Au <sub>1</sub> Sn <sub>1</sub> /CNT	0.5 M H <sub>2</sub> SO <sub>4</sub> + 1 M CH <sub>3</sub> OH	49.3	0.49	50	14
PtPdCu nanodendrites	0.5 M H <sub>2</sub> SO <sub>4</sub> + 1 M CH <sub>3</sub> OH	75	0.52	50	15
Ag <sub>4</sub> Au <sub>1</sub> Pt <sub>2</sub> /MWCNTs	0.5 M H <sub>2</sub> SO <sub>4</sub> + 2 M CH <sub>3</sub> OH	N. A	0.152	50	16

Pt <sub>3</sub> Bi <sub>3</sub> Zn NPLs	0.1 M HClO <sub>4</sub> + 0.5 M CH <sub>3</sub> OH	109.3	3.29	20	17
Pt-on-Pd/Ti <sub>3</sub> C <sub>2</sub> Tx	0.5 M H <sub>2</sub> SO <sub>4</sub> + 1 M CH <sub>3</sub> OH	157.3	0.922	50	18

### Reference:

- 1 F. Chen, C. Yu, J. Cui, D. Yu, P. Song, Y. Wang, Y. Qin, J. Yan and Y. Wu, *Appl Surf Sci*, 2021, **541**, 148473.
- 2 Y. Sun, C. Du, G. Han, Y. Qu, L. Du, Y. Wang, G. Chen, Y. Gao and G. Yin, *Electrochim Acta*, 2016, **212**, 313–321.
- 3 Y. Ren, K. Chen, Y. Zhang, D. Shi, Q. Wu, D. Liang, C. Hu and H. Li, *J Mater Chem A Mater*, 2022, **10**, 13345–13354.
- 4 T. Wang, J. He, Q. Wu, Y. Yu, K. Chen, D. Shi, Y. Zhang and H. Li, *Carbon N Y*, 2023, **201**, 200–211.
- 5 P. Deshpande and B. L. V. Prasad, *ACS Appl Mater Interfaces*, 2023, **15**, 26554–26562.
- 6 C. Koenigsmann, A. C. Santulli, K. Gong, M. B. Vukmirovic, W. Zhou, E. Sutter, S. S. Wong and R. R. Adzic, *J Am Chem Soc*, 2011, **133**, 9783–9795.
- 7 L. Feng, K. Li, J. Chang, C. Liu and W. Xing, *Nano Energy*, 2015, **15**, 462–469.
- 8 K. Bhunia, S. Khilari and D. Pradhan, *Dalton Transactions*, 2017, **46**, 15558–15566.
- 9 X. Chen, H. Wang, Y. Wang, Q. Bai, Y. Gao and Z. Zhang, *Catalysts*, 2015, **5**, 1003–1015.

- 10 Y. Yang, L.-M. Luo, R.-H. Zhang, J.-J. Du, P.-C. Shen, Z.-X. Dai, C. Sun and X.-W. Zhou, *Electrochim Acta*, 2016, **222**, 1094–1102.
- 11 S. Jiang, B. Yi, Q. Zhao, H. Zhang, Y. Su, H. Yu and Z. Shao, *RSC Adv*, 2016, **6**, 82370–82375.
- 12 W. Liu, P. Wang and Z. Wang, *CrystEngComm*, 2021, **23**, 7978–7984.
- 13 Y. Lu, W. Wang, X. Chen, Y. Zhang, Y. Han, Y. Cheng, X.-J. Chen, K. Liu, Y. Wang, Q. Zhang and S. Xie, *Nano Res*, 2019, **12**, 651–657.
- 14 B. Singh, L. Murad, F. Laffir, C. Dickinson and E. Dempsey, *Nanoscale*, 2011, **3**, 3334.
- 15 P. Wang, Y. Zhang, R. Shi and Z. Wang, *ACS Appl Energy Mater*, 2019, **2**, 2515–2523.
- 16 K. Thongthai, P. Pakawanit, N. Chanlek, J.-H. Kim, S. Ananta and L. Srisombat, *Nanotechnology*, 2017, **28**, 375602.
- 17 H. Tian, D. Wu, J. Li, J. Luo, C. Jia, Z. Liu, W. Huang, Q. Chen, C. M. Shim, P. Deng, Y. Shen and X. Tian, *Journal of Energy Chemistry*, 2022, **70**, 230–235.
- 18 C. Yang, Q. Jiang, H. Liu, L. Yang, H. He, H. Huang and W. Li, *J Mater Chem A Mater*, 2021, **9**, 15432–15440.